

Carbon monoxide (CO) vertical profiles derived from joined TES and MLS measurements

Ming Luo,¹ William Read,¹ Susan Kulawik,¹ John Worden,¹ Nathaniel Livesey,¹ Kevin Bowman,¹ and Robert Herman¹

Received 21 June 2014; revised 26 August 2013; accepted 29 August 2013.

[1] TES (Tropospheric Emission Spectrometer) nadir and MLS (Microwave Limb Sounder) limb measurements from the Aura satellite are used to jointly estimate an atmospheric carbon monoxide (CO) profile with extended vertical range compared to profiles retrieved from the individual measurement. We describe the algorithms, the processing procedures, the prototyping results, and the evaluations for this new joint product. TES and MLS “stand-alone” CO profile retrievals are largely complementary, with TES being largely sensitive to lower to middle troposphere while MLS measures CO in the upper troposphere and above. We pair TES nadir and MLS limb tangent locations within 6–8 min and within 220 km. The paired radiance measurements of the two instruments in each location are optimally combined to retrieve a single CO profile along with other trace gases whose signal interferes with that from CO. This combined CO profile has a vertical resolution and vertical range that is an improvement over the two stand-alone products, especially in the upper troposphere/lower stratosphere. For example, the degrees of freedom for signal (DOFS) between surface and 50 hPa for TES alone are < 2 , and for the combined CO profiles are 2–4. This new Aura CO product will be made available to the public using TES V005 and MLS V003 processing results and will provide a unique data set for studying tropospheric transport of air pollutants and troposphere-stratospheric exchange processes.

Citation: Luo, M., W. Read, S. Kulawik, J. Worden, N. Livesey, K. Bowman, and R. Herman (2013), Carbon monoxide (CO) vertical profiles derived from joined TES and MLS measurements, *J. Geophys. Res. Atmos.*, 118, doi:10.1002/jgrd.50800.

1. Introduction

[2] Recent satellite measurements of atmospheric constituents provide global and multiyear data sets for use in advancing knowledge of tropospheric and stratospheric chemical and dynamical processes (e.g., NASA’s Earth Observing System and ESA’s Earth Observing missions). These observations include relatively short-lived species with significant anthropogenic sources, such as carbon monoxide (CO), nitrogen dioxide (NO₂), ozone (O₃), and ammonia (NH₃); they also include long-lived greenhouse gases, e.g., carbon dioxide (CO₂) and methane (CH₄). These products are characterized by pressure-dependent information parameters. For the thermal infrared nadir observations, the effective gas absorption occurs in the troposphere. The knowledge gained in the species profiles is therefore limited to the troposphere. In contrast, satellite limb observations provide rich knowledge of the species vertical distributions in the upper troposphere and above with vertical resolution defined, in part, by their field-of-view at the limb. The algorithm described here combines nadir infrared measurements from the Tropospheric

Emission Spectrometer (TES) and the limb measurements from the Microwave Limb Sounder (MLS) on the NASA Aura satellite to derive carbon monoxide (CO) profiles with sensitivities from the surface to ~90 km.

[3] Carbon monoxide is one of the key trace gases in the Earth’s atmosphere relating air quality and climate systems. The oxidation of CH₄ and other hydrocarbons provides a uniform background for CO. Incomplete combustions of fossil fuels and biomass are strong anthropogenic sources of CO. Forest fires also release CO in the atmosphere. CO reacts with hydroxyl radical (OH) as its removal mechanism. It is therefore an important precursor for tropospheric ozone production via series chemical reactions in the presence of NO_x [Logan *et al.*, 1981]. With a lifetime of weeks, the global seasonally dependent CO distributions near the surface and in the lower troposphere exhibit obvious highs over the emission sources and tracks of enhanced CO in the downwind regions [Zhang *et al.*, 2006; Jiang *et al.*, 2007]. CO is also an excellent tracer for convective processes [Li *et al.*, 2005; Schoeberl *et al.*, 2008; Gonzi and Palmer, 2010; Luo *et al.*, 2010; Liu *et al.*, 2010; Pumphrey *et al.*, 2011; Zhang *et al.*, 2011]. Measurements of CO vertical profiles from troposphere to lower stratosphere with vertical independent pieces of information greater than two are therefore very useful in linking sources and transport pathways of pollutants and improving knowledge on ozone production in the troposphere and how air exchanges between the troposphere and stratosphere.

¹Jet Propulsion Laboratory, California Institute of Technology, Pasadena, California, USA.

Corresponding author: M. Luo, Jet Propulsion Laboratory, California Institute of Technology, Pasadena, CA 91109, USA. (Ming.Luo@jpl.nasa.gov)

©2013. American Geophysical Union. All Rights Reserved.
2169-897X/13/10.1002/jgrd.50800

[4] Global measurements of tropospheric CO have become available in recent decades from several nadir-looking satellite instruments: MOPITT (Measurements of Pollution in the Troposphere) on the Terra spacecraft [Edwards *et al.*, 2004], SCIAMACHY (Scanning Imaging Spectrometer for CHartographY) on ENVISAT [Bovensmann *et al.*, 1999], AIRS (Atmospheric Infrared Sounder) on the Aqua satellite [Aumann *et al.*, 2003], TES on Aura satellite [Beer *et al.*, 2001], and IASI (Infrared Atmospheric Sounding Interferometer) on MetOp satellite [George *et al.*, 2009]. These observations provide tropospheric CO with less than two pieces of independent layer information in the troposphere. Satellite limb observations are obtained with solar occultation instrument ACE (Atmospheric Chemistry Experiment) on SCISAT-1 [Barret *et al.*, 2005] and in emission by MLS (Microwave Limb Sounder) on Aura satellite [Filipiak *et al.*, 2005; Waters *et al.*, 2006]. These limb observations provide CO profiles from upper troposphere to mesosphere with high vertical resolution in the order of 3–4 km. CO data from nadir observations, sensitive to the lower-middle troposphere, and limb observations sensitive to upper troposphere and above, are used in studies of troposphere-stratosphere exchange processes and model chemistry-transport evaluation [Logan *et al.*, 2008; Nassar *et al.*, 2009; Luo *et al.*, 2010; Liu *et al.*, 2010].

[5] Here we report a new algorithm that combines TES and MLS measured radiance spectra to retrieve CO profiles with sensitivities from the lower troposphere to the mesosphere. We also report preliminary results from the application of this algorithm to TES and MLS observations. The nadir looking TES and limb looking MLS instruments are both on the NASA Aura satellite. Although their nadir and tangent footprints are not exactly colocated, the same orbital observations still provide ideal data sets for this experiment. Section 2 of this work describes TES and MLS instruments. Section 3 details the measurement pairing approach, the algorithm for CO profile retrieval with joint radiance measurements, and the characteristics of the results. Section 4 describes a 1 day example for the combined CO retrieval. Section 5 evaluates a TES-MLS CO profile by comparing it to an AirCore in situ measurement. Finally, section 6 provides a summary of this work and outlines future plans.

2. TES and MLS CO Observations

[6] TES and MLS are two of the four instruments onboard NASA’s Aura satellite launched in July 2004 [Schoeberl *et al.*, 2006]. Aura is in a sun-synchronous polar orbit with a 98° inclination angle and the equator ascending crossing at about 1:45 P.M. local time. Aura orbits the earth at 705 km with about 14.5 orbits per day. MLS looks forward and scans vertically to obtain emission spectra at the limb. When in “Global Survey” mode or the “Step and Stare” and some “Transect” special observation mode, TES takes nadir spectral measurements along Aura orbits. TES nadir footprints and MLS limb tangent locations are separated by 7 ± 0.3 min and 50–220 km, with MLS tangent points lying to the east of the TES nadir observations due to Earth’s rotation. Accordingly, TES and MLS spectral radiance measurements are not ideally colocated. However, since MLS limb measurements provide information to the joint CO profile retrieval only in the upper troposphere and above, this mismatch should have minimum effects in most cases,

but it does need to be borne in mind when using the combined CO data in regions of strong horizontal gradients.

[7] TES is an infrared Fourier transform spectrometer covering 650–3050 cm^{-1} with spectral resolution of 0.1 cm^{-1} for the nadir-viewing mode [Beer, 2006]. This high spectral resolution allows TES to obtain spectral measurements of weak absorption lines and therefore to retrieve vertically resolved profiles of atmospheric species, e.g., ozone and CO in the lower to middle troposphere. The TES footprint is about 5×8 km at nadir, small enough to provide cloud-free measurements in most cases. In addition to “Special Observations” scheduled for special events or observation campaigns, the main TES operational mode is nadir “Global Survey” (GS). TES GSs are taken every other day for successively 16 orbits (~ 26 h). Over the mission period since 2004, TES GS latitude coverage and distance between the adjacent footprints were changed a few times in order to conserve instrument lifetime. Detailed description of these observation strategy modifications can be found in “TES Level 2 Data User’s Guide” [Herman and Kulawik, 2013].

[8] TES CO products have been validated by comparisons to other satellite data and the in situ observations [Luo *et al.*, 2007a, 2007b; Lopez *et al.*, 2008; Ho *et al.*, 2009]. TES CO are found negatively biased by less than 10%. The current version V005 data differ from the previous version merely due to the usage of different a priori [Herman and Osterman, 2012]. Enhancements in TES CO data in the lower to upper troposphere have been seen associated with emission sources, e.g., biomass-burning regions and forest fires, and their downwind pathways. As an example, Figure 1 shows TES CO volume mixing ratio (VMR) at 215 hPa taken 9–10 Feb 2009 Global Survey. The high CO values in the tropical latitudes reflect large-scale upwelling processes in the vicinity of biomass burning regions, e.g., south-central Africa. Prior to TES GS observations on this day, a large bush fire occurred in southeast Australia [Pumphrey *et al.*, 2011; Siddaway and Petelina, 2011; de Laat *et al.*, 2012; Glatthor *et al.*, 2013]. TES CO enhanced VMRs at a few observation locations along the Aura orbits are seen to the east of the Australia source region in 9–10 Feb 2009 data. As shown below, MLS CO data also indicate the upper-tropospheric CO enhancement to the east of Australia.

[9] MLS is a limb viewing radiometer that measures atmospheric emission spectra from the 230 GHz CO rotational lines as its field of view is scanned through the atmosphere. The spectra are used in an optimal estimation approach to retrieve a CO concentration profile from 300 hPa into the mesosphere [Livesey *et al.*, 2006; Pumphrey *et al.*, 2007].

[10] MLS CO profile retrievals are useful in scientific research at pressures of 215 hPa and less [Livesey *et al.*, 2011]. Comparisons to in situ validation data indicated that the MLS CO VMRs were about 2 times higher at 215 hPa in the V2.2 data set [Livesey *et al.*, 2008]. The newly released V3.3 data are much improved. The main improvement is that the background absorption is changed from a spectrally flat extinction quantity to relative humidity extinction. The relative humidity extinction quantity has a frequency squared dependence that better models the spectral dependence of the background absorption [Livesey *et al.*, 2011]. Figure 2 shows MLS CO VMRs at 215 hPa, selected to match (as described in the following section) with TES GS observations shown in Figure 1 on 9–10 Feb 2009. Compared to TES CO data

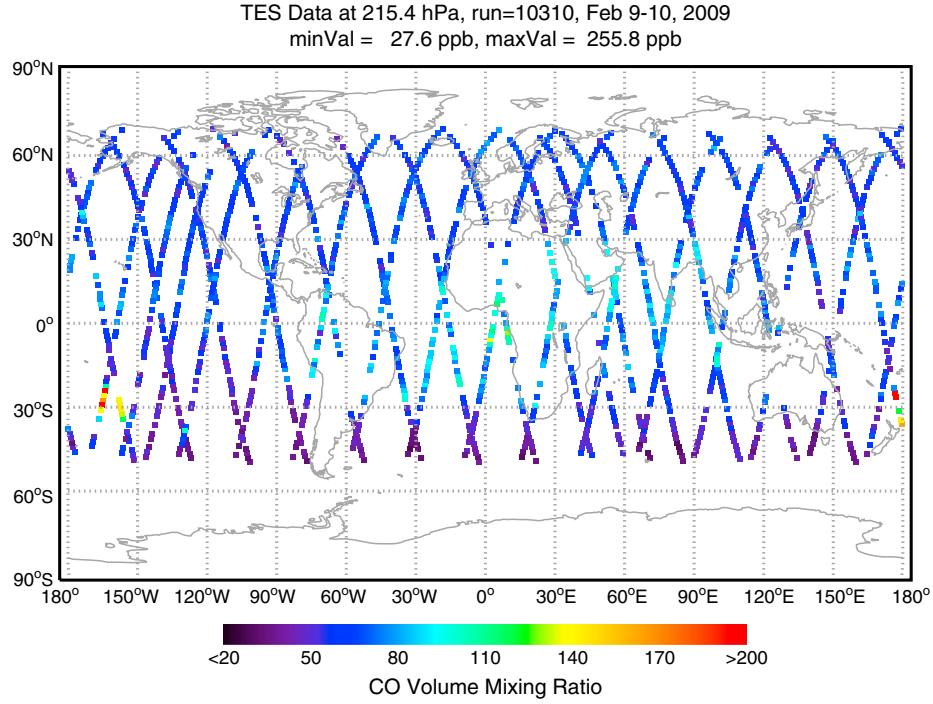


Figure 1. TES Global Survey CO retrievals at 215 hPa for 9–10 February 2009. Each symbol shows the location of the TES nadir footprint.

(Figure 1), MLS CO data show higher variability at 215 hPa. This variability reflects a combination of the greater sensitivity of MLS to the upper troposphere and the noise on individual MLS observations. Such noise can be reduced by introducing tighter retrieval constraints (e.g., stronger horizontal and/or vertical smoothing terms in the optimization). As seen in the TES

CO global distributions, MLS also show high CO abundances in the upwelling tropical region and in the vicinity of the known SE Australia bush fire sources. Figure 3 shows the histogram of TES and MLS CO VMRs at 215 hPa. They agree well in value distributions where TES values are all positive due to the lnVMR retrieval [Bowman *et al.*, 2006].

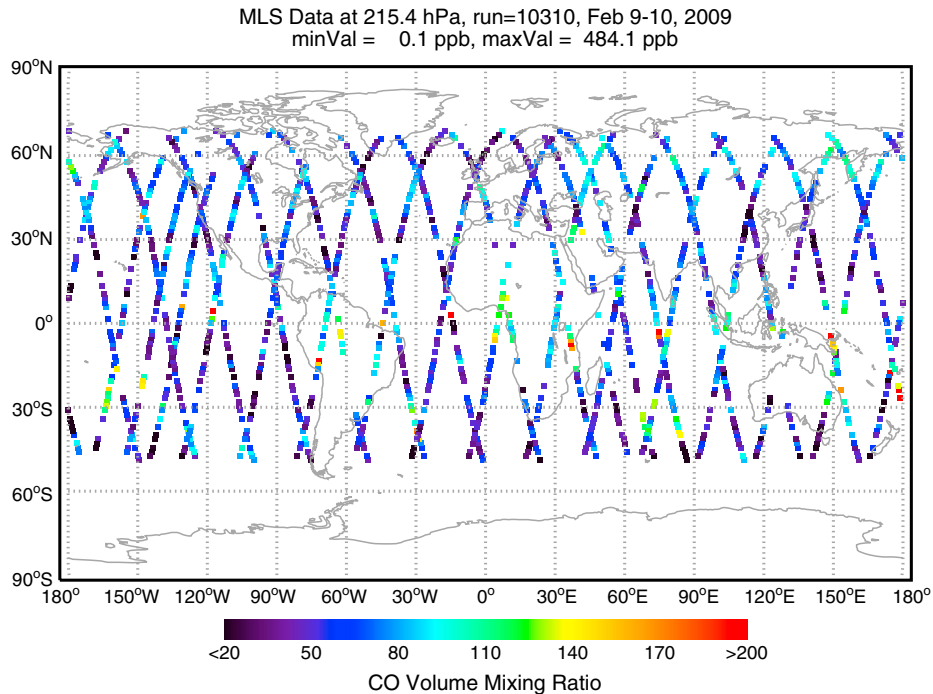


Figure 2. MLS CO retrievals at 215 hPa selected to match to TES Global Survey data taken 9–10 February 2009 shown in Figure 1.

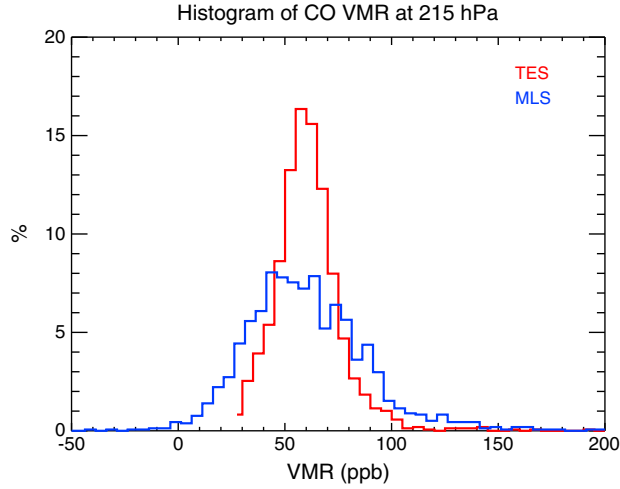


Figure 3. Normalized histograms of TES and MLS CO retrievals at 215 hPa from data taken 9–10 February 2009 shown in Figures 1 and 2, respectively. For TES, the mean and the standard deviation for CO VMRs are 62 and 15.4 ppb, respectively; for MLS, the mean and standard deviation for CO VMRs are 63 and 33 ppb, respectively.

3. Algorithms and Strategies for Producing the TES-MLS Joint CO Product

3.1. TES Nadir and MLS Tangent Location/Time Pairing

[11] TES and MLS observations are pair-matched based on time and location. Since TES GS operates on a 1 day-on followed by 1 day-off mode and MLS operates continuously,

we find the closest MLS tangent location for each TES nadir location. We first select TES and MLS CO data with good quality flags. The TES data are selected using the Master Quality flag based on several criteria, e.g., the influence of the cloud in the retrieval [Herman and Kulawik, 2013]; the MLS data are selected using “Precision,” “Status (radiance fits),” “Clouds,” etc. criteria [Livesey et al., 2011]. For a given TES location, the MLS data are limited to within 6–8 min of the TES observation; we then select the MLS matching location closest to the TES location.

[12] Figure 4 shows the TES and MLS geolocations for their matched pairs in TES Global Survey day 9–10 Feb 2009. Most of the missing data along orbits are due to quality screening of TES CO data. Figure 5 shows the time differences and the distances between TES-MLS matched pairs. An MLS tangent is always ahead of its matching TES nadir location by about 7 min. The distance between the two locations varies from about 50 km at high latitudes to about 200 km near the equator with 20 km variability in given latitude. This separation should be taken into consideration when an interesting feature in CO distribution is small or with large horizontal gradients. In the selection procedure, we remove the TES-MLS pairs with distances greater than 220 km.

3.2. Optimal Retrieval of CO Profile

[13] TES nadir spectral radiances in 11 microwindows in 2086–2165 cm^{-1} and MLS spectral radiances in GHz “Band 9” (centered on the 230.5 GHz CO line) are used to retrieve a common CO profile for a given matched TES-MLS measurement pair. MLS measurement in “Band 8” is a candidate for future addition. Optimal estimation theory [Rodgers, 2000] is used for retrieving the state vector \mathbf{x} (e.g., the

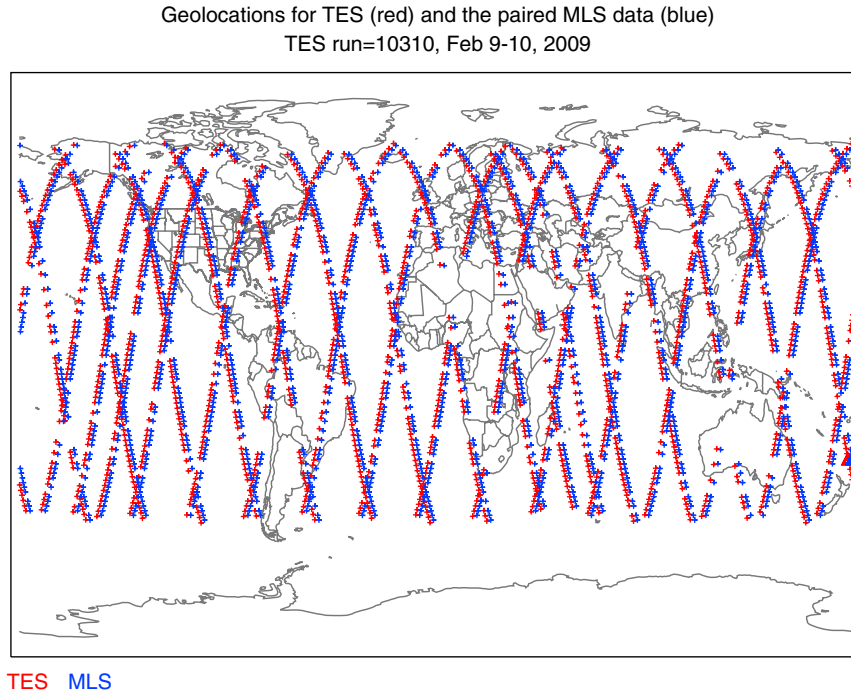


Figure 4. TES nadir geolocations (blue) and MLS tangent locations (red) matched for a TES Global Survey on 9–10 Feb 2009. The triangle symbols to the east of Australia are TES and MLS locations for an example scene described in Figures 7 and 13.

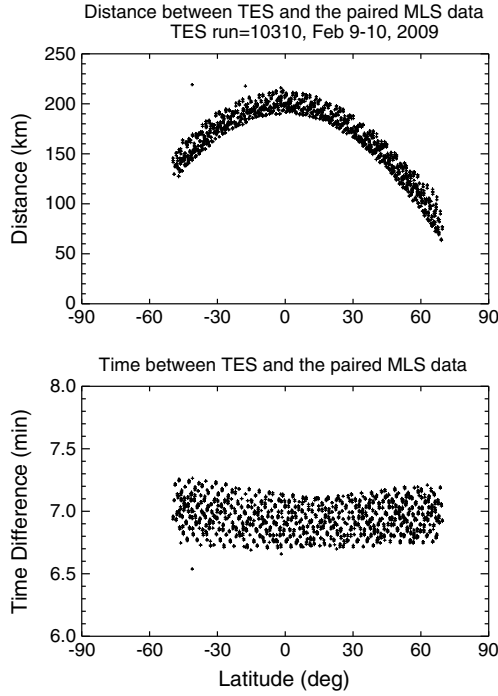


Figure 5. (top) The distances in kilometers and (bottom) the time differences in minutes between TES and MLS matched observation pairs shown in Figure 4 for 9–10 Feb 2009.

profiles for CO and other species with absorption features in the selected spectral band), according to

$$\mathbf{x}^{i+1} = \mathbf{x}^i + \hat{\mathbf{S}}_t \left[\mathbf{K}_{\text{TES}}^T \mathbf{S}_{y_{\text{TES}}}^{-1} (\mathbf{y}_{\text{TES}} - \mathbf{FM}_{\text{TES}}(\mathbf{x}^i)) + \mathbf{K}_{\text{MLS}}^T \mathbf{S}_{y_{\text{MLS}}}^{-1} (\mathbf{y}_{\text{MLS}} - \mathbf{FM}_{\text{MLS}}(\mathbf{x}^i)) + \mathbf{S}_a^{-1} (\mathbf{x}_a - \mathbf{x}^i) \right] \quad (1)$$

where i is the iteration number, \mathbf{K} represent Jacobians (the sensitivity of measurement radiance to the state vector, \mathbf{x} ,

$\partial \text{Radiance} / \partial \mathbf{x}$), \mathbf{FM} represents the forward model calculated radiance, \mathbf{y} is the measured radiance, \mathbf{S}_y is the measurement noise, \mathbf{x}_a and \mathbf{S}_a are the a priori constraint vector and covariance, respectively.

[14] The total retrieval error ($\hat{\mathbf{S}}_t$) and the averaging kernel (\mathbf{A}) are calculated by the following equations 2 and 3.

$$\hat{\mathbf{S}}_t = \left(\mathbf{K}_{\text{TES}}^T \mathbf{S}_{y_{\text{TES}}}^{-1} \mathbf{K}_{\text{TES}} + \mathbf{K}_{\text{MLS}}^T \mathbf{S}_{y_{\text{MLS}}}^{-1} \mathbf{K}_{\text{MLS}} + \mathbf{S}_a^{-1} \right)^{-1} \quad (2)$$

$$\mathbf{A} = \hat{\mathbf{S}}_t \left(\mathbf{K}_{\text{TES}}^T \mathbf{S}_{y_{\text{TES}}}^{-1} \mathbf{K}_{\text{TES}} + \mathbf{K}_{\text{MLS}}^T \mathbf{S}_{y_{\text{MLS}}}^{-1} \mathbf{K}_{\text{MLS}} \right) \quad (3)$$

[15] TES forward model calculations are avoided to reduce processing time by assuming that the TES forward model is linearly related to the state vector, $\mathbf{FM}_{\text{TES}}(\mathbf{x}_{\text{ret_TES}}) = \mathbf{FM}_{\text{TES}}(\mathbf{x}^i) + \mathbf{K}_{\text{TES}}(\mathbf{x}_{\text{ret_TES}} - \mathbf{x}^i)$, where $\mathbf{x}_{\text{ret_TES}}$ is TES retrieved state. Substituting this relation to equation 1, the combined retrieval equation becomes

$$\begin{aligned} \mathbf{x}^{i+1} = \mathbf{x}^i + \hat{\mathbf{S}}_t \left[\mathbf{K}_{\text{TES}}^T \mathbf{S}_{y_{\text{TES}}}^{-1} (\mathbf{y}_{\text{TES}} - \mathbf{FM}_{\text{TES}}(\mathbf{x}_{\text{ret_TES}})) \right. \\ \left. + \mathbf{K}_{\text{TES}}^T \mathbf{S}_{y_{\text{TES}}}^{-1} \mathbf{K}_{\text{TES}} (\mathbf{x}_{\text{ret_TES}} - \mathbf{x}^i) \right. \\ \left. + \mathbf{K}_{\text{MLS}}^T \mathbf{S}_{y_{\text{MLS}}}^{-1} (\mathbf{y}_{\text{MLS}} - \mathbf{FM}_{\text{MLS}}(\mathbf{x}^i)) + \mathbf{S}_a^{-1} (\mathbf{x}_a - \mathbf{x}^i) \right] \quad (4) \end{aligned}$$

[16] Two TES terms (a vector and a matrix) in the above equation can be prestored for each profile, $\mathbf{K}_{\text{TES}}^T \mathbf{S}_{y_{\text{TES}}}^{-1} (\mathbf{y}_{\text{TES}} - \mathbf{FM}_{\text{TES}}(\mathbf{x}_{\text{ret_TES}}))$ and $\mathbf{K}_{\text{TES}}^T \mathbf{S}_{y_{\text{TES}}}^{-1} \mathbf{K}_{\text{TES}}$. Beginning in TES Version 005 processing, the outputs of these two terms per profile are implemented in the Level 2 processing at its final iteration step for CO. In the TES retrieval system, the Jacobian (\mathbf{K}_{TES}) are calculated treating the state vector as lnVMR. It is converted analytically to treating the state vector as VMR for the TES-MLS algorithm described here.

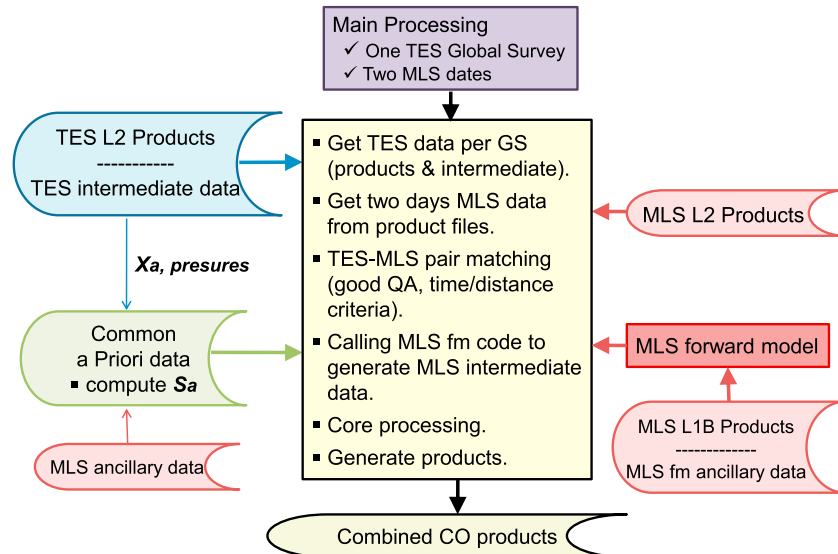


Figure 6. Top level processing flowchart for TES-MLS jointly retrieved CO product.

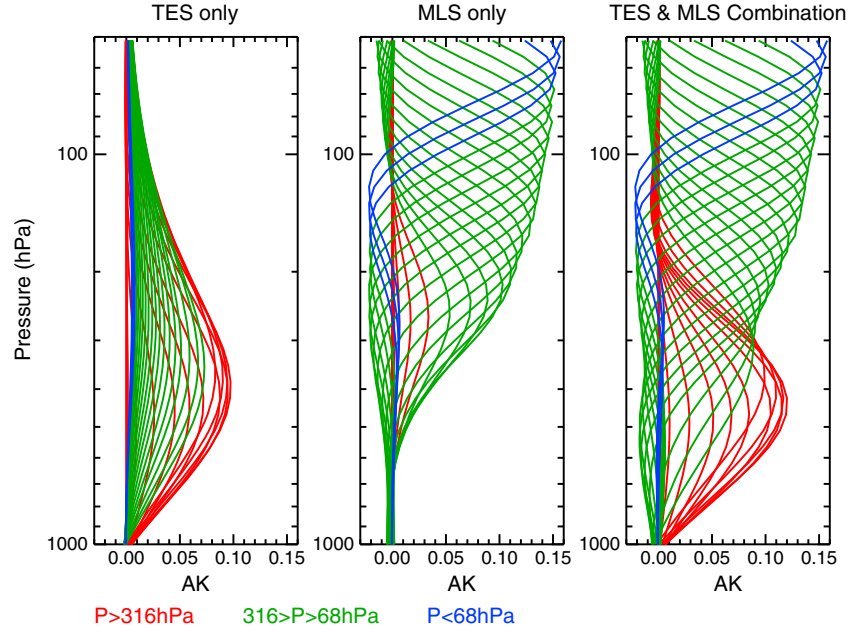


Figure 7. Averaging Kernel (AK) plots for CO profile retrievals from TES measurements only, MLS measurements only and TES-MLS measurement combination cases. The measurements' geolocation is shown in Figure 4. Common a priori constraint is used.

[17] In the MLS Level2 processing algorithm, species retrievals are done in two dimensions for the Aura orbital plane, including the CO profile retrieval [Livesey *et al.*, 2006]. Here we use MLS limb measurements taken at a single vertical-scan frame closest to the L2 reported tangent location, and ignore the impact of horizontal gradients in CO and other species in the observed radiances. In this new retrieval, together with TES measurements, some other species that contribute to the radiance absorption in MLS GHz Band 9 are retrieved simultaneously with CO. These parameters include ozone, and background extinction profiles which are used to account for both dry and moist continuum absorption. In equation 4, a stand-alone MLS forward model is executed to calculate the model radiance with the MLS retrieved forward model species as initial guesses. MLS limb radiances taken above 316 hPa are used in the combined retrieval.

[18] For the combined TES-MLS CO retrieval, we adopt the numerical treatment of scaling the radiances by S_y^{-1} and the state vector (VMR) by the a priori error in equations 2–4 described in MLS algorithm [Livesey *et al.*, 2006]. The common a priori constraint profile is the same as that used in TES [Herman and Kulawik, 2013]. The common constraint matrix (S_a) for CO follows that of MLS [Livesey *et al.*, 2006] but modified

tighter for pressure levels at and greater than 100 hPa so the effect in the retrieved profile is similar to that in TES retrievals in the troposphere. All retrievals are performed at TES forward model pressure levels from surface to 0.1 hPa (equal or fewer than 67 levels depending on the surface pressure).

[19] To briefly summarize the TES-MLS joint CO retrieval process, Figure 6 shows the top-level flow diagram. For each TES Global Survey of about 26 h, 2 days of MLS data are identified. The first step in the process is to match TES-MLS observation pairs described in section 3.1 above. The process then gathers the required MLS data and the initial guess for CO (e.g., TES climatology) and calls the MLS forward model to compute model radiance, and Jacobians for CO and other retrieval parameters. TES product data and the prestored terms are also made available. Equation 4 is then

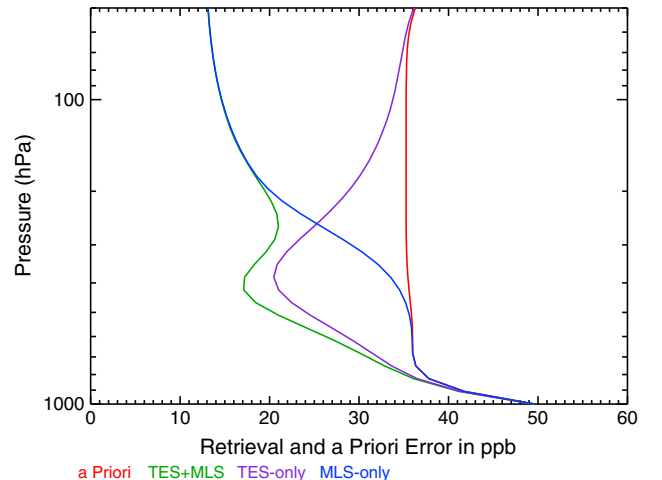


Figure 8. Profiles for the a priori and retrieval errors. Same case as in Figure 7.

Table 1. DOFS and Information Content Calculated for the Selected Pressure Ranges

	TES-Only	MLS-Only	TES-MLS Combined
DOFS (total)	1.51	12.4	13.3
DOFS (surface–150 hPa)	1.02	0.71	1.57
DOFS (400–100 hPa)	0.67	1.4	1.7
Info Content (total)	2.0	25	26.6
Info Content (Surf–150 hPa)	1.3	0.5	1.9
Info Content (400–100 hPa)	0.5	1.3	1.6

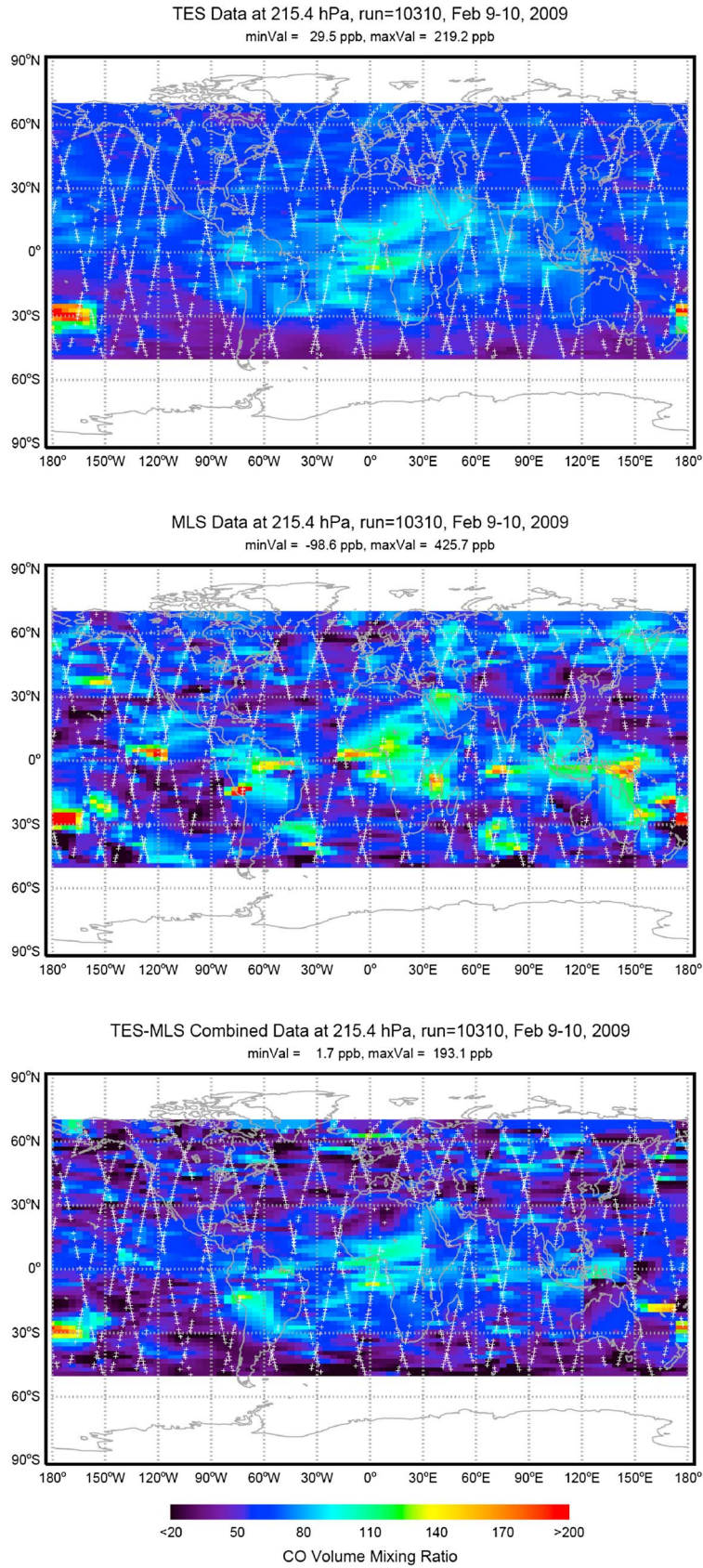


Figure 9. CO VMR global distribution at 215 hPa for 9–10 Feb 2009: (top) TES CO product, (middle) MLS CO product, and (bottom) TES-MLS combined CO product. TES (Figures 9, top and 9, bottom) and MLS (9, middle) geolocations are marked by white “plus” symbols. VMR values at those observation locations are interpolated horizontally.

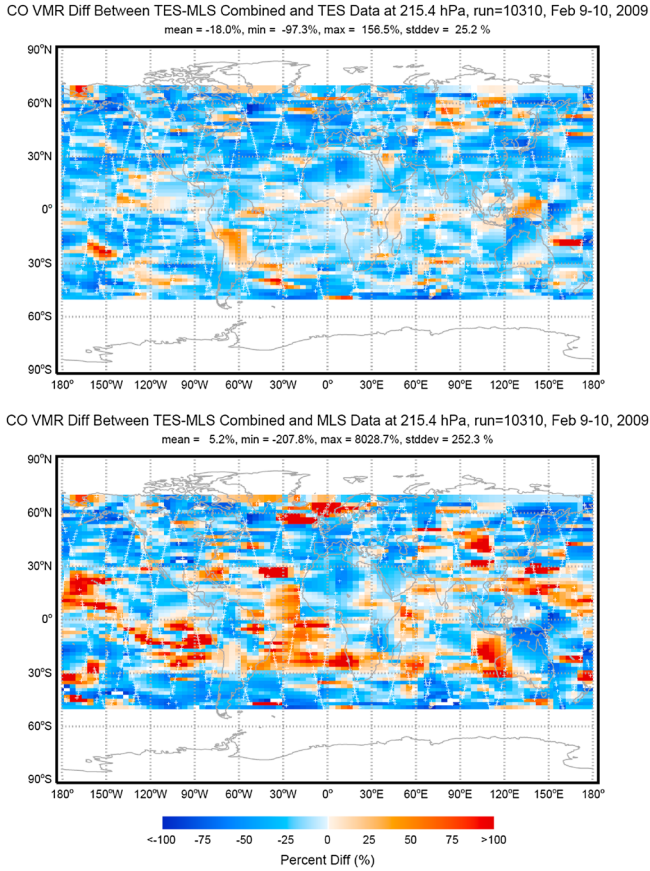


Figure 10. CO VMR differences at 215 hPa (top) between TES-MLS combined and TES data and (bottom) between TES-MLS combined and MLS data for 9–10 Feb 2009.

used to retrieve the common CO profile covering the entire atmosphere and other MLS GHz Band 9 related species. The retrieved CO profiles are then archived in a HDF-EOS5 file in the same manner as measurements from the TES Global Surveys. The averaging kernels (equation 3) and total retrieval errors (equation 2) along with TES and MLS geolocation information are also provided in the output files.

3.3. MLS Callable Forward Model

[20] The MLS team has produced an interface that allows the MLS “callable” forward model (CFM) to be executed from other software drivers such as the retrieval module described here. The CFM added necessary flexibility to accomplish this task. The CFM produces radiances and Jacobians with respect to species and temperature in the state vector. Since the CFM accepts flexible inputs, the following issues were most easily circumvented by directly calling the CFM rather than using preexisting tables and results as is being done by TES: (1) the individual retrieval grids used by MLS and TES in their standard processing are different and needed to be the same for the joint retrieval, and (2) the lowest retrieval grid point changes depending on surface topography. The algorithm of the CFM is described by *Read et al.* [2006].

3.4. Characterizing the Jointly Retrieved CO Profile

[21] Here we use a single profile case to describe and illustrate the characteristics of a TES and MLS jointly retrieved

CO profile, comparing to the stand-alone retrievals that use either TES or MLS measurements alone. We consider the averaging kernels and the degree of freedom for signal (DOFS) characterizing the vertical resolution and the extent of the retrievals, the retrieval errors compared to the a priori error, and the Shannon information content defining change of knowledge on the state after making the measurements [Rodgers, 2000]. The common profile constraint (\mathbf{x}_a) in VMR is the same as that used by the TES team and the common constraint matrix (\mathbf{S}_a) is the same as that used by the MLS team modified at pressure levels between 100 hPa and the surface to reduce the variability in the retrieval. The example profile retrieval is for the case taken from the 10 Feb 2009 measurements located to the east of Australia shown in Figure 4.

[22] Figure 7 shows the averaging kernels of surface to lower stratosphere for TES and MLS only and their combined retrievals. TES-only AKs peak around 400 hPa. MLS-only AKs are effective from ~ 300 hPa to the stratosphere. The TES-MLS combined AKs show the sensitivity that covers both TES and MLS sensitive regions. Compared to TES-only or MLS-only cases, the TES-MLS combined retrievals gain sensitivity in upper troposphere and above and middle troposphere, respectively.

[23] The DOFS quantifies the AKs. It describes the number of independent parameters in the retrieved profile. The Shannon information content also describes the gain with the measurement from the a priori knowledge [Rodgers, 2000]. Table 1 lists the calculated DOFS and the information content for TES and MLS-only and their combined CO profile retrievals for selected pressure ranges that cover troposphere to lower stratosphere. As illustrated in Figure 7, TES-only and MLS-only CO retrievals are sensitive in different vertical ranges in the atmosphere, and their jointly retrieved CO combine information from the two instruments that extend from surface to the stratosphere.

[24] Finally, the retrieval errors corresponding to TES and MLS-only and the combined CO retrievals are shown in Figure 8. The common a priori error profile (the square roots of the diagonals of the constraint matrix) used for generating TES-MLS CO products is also shown. For this case (southern hemispheric ocean), compared to the a priori error of about 36 ppb, the TES-only retrieval error is in a layer of 700–150 hPa with minimum of ~ 20 ppb at 400 hPa; the MLS-only retrieval error greatly reduce the a priori at ~ 250 hPa and less. The retrieval errors in TES and MLS combined CO profile are the minimum of the two stand-alone retrievals.

4. Retrieval Example

[25] Here we illustrate the TES-MLS joint retrieved CO product for 9–10 Feb 2009. Figures 9 and 11 show the original TES and MLS and the combined CO distributions at 215 and 681 hPa, respectively. TES (top and bottom panels) and MLS (middle panel) geolocations are marked with “plus” symbols. CO VMRs at those locations are interpolated horizontally for better visualization purposes.

[26] At 215 hPa (Figure 9), the TES CO distribution shows similar features to those in the a priori (not shown), e.g., enhancements in some tropical regions due to strong convection that brings up air with enhanced CO concentrations emitted by biomass burning. However, very high CO concentrations

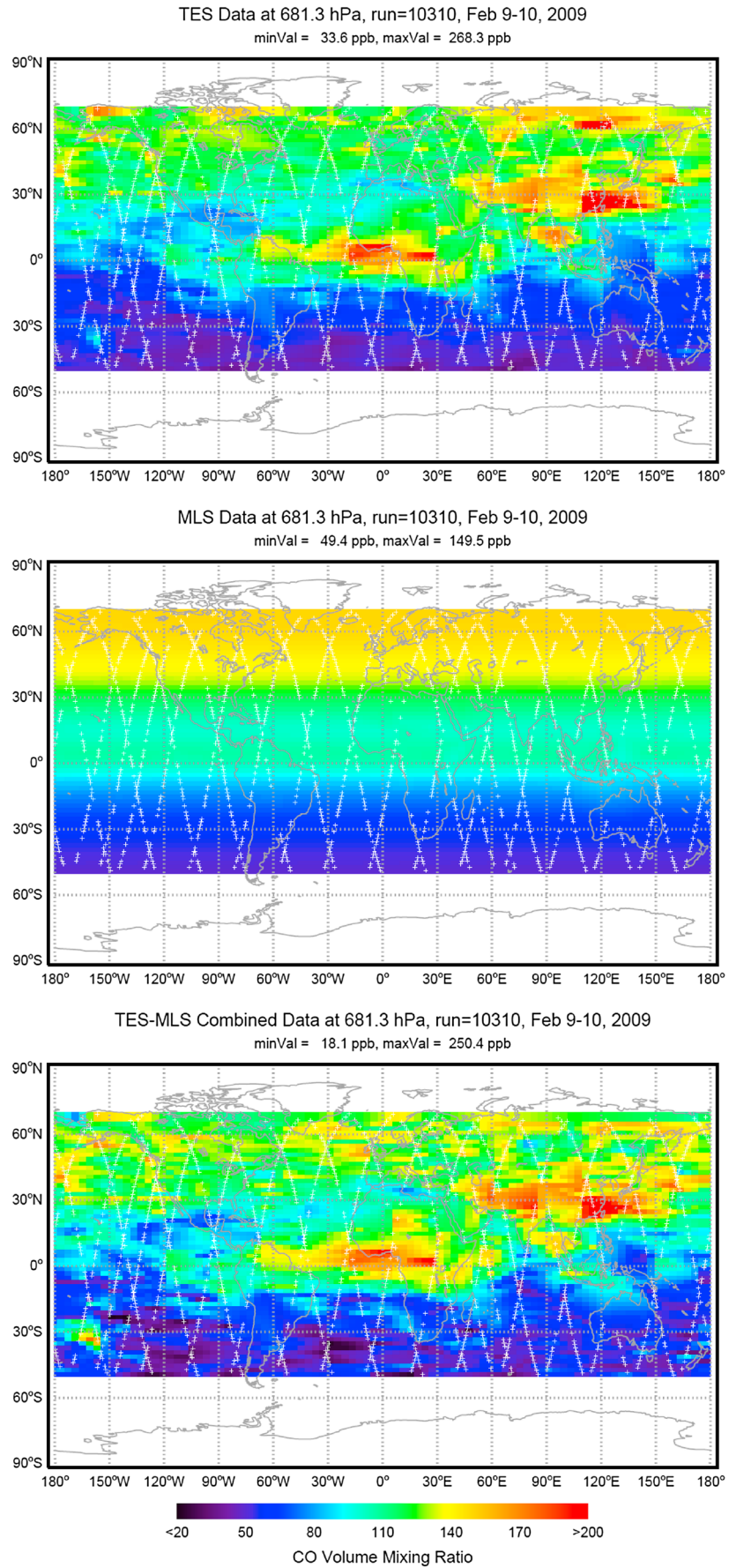


Figure 11. Same as Figure 9 but at 681 hPa.

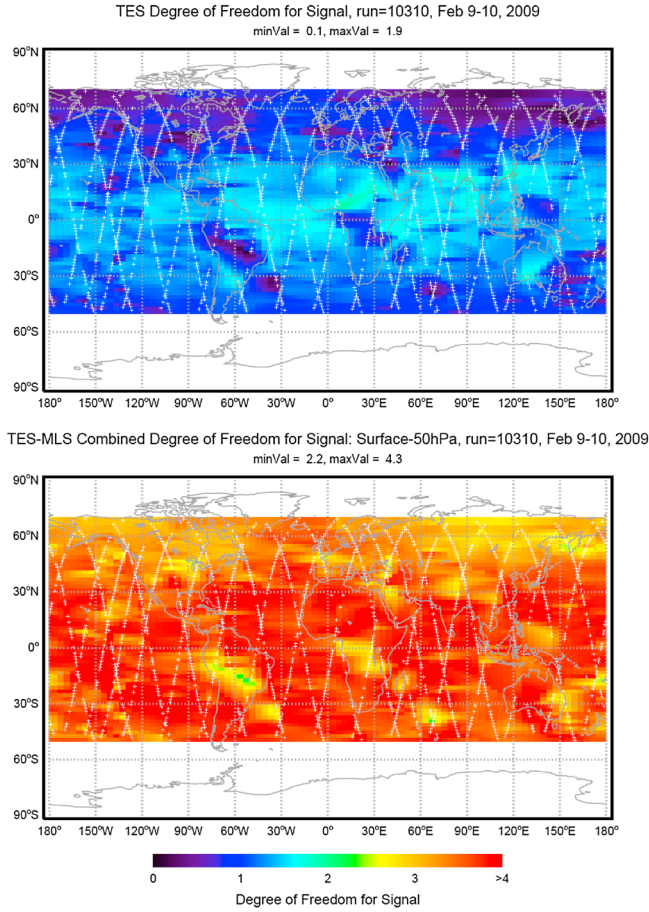


Figure 12. The degree of freedom for signal (DOFS) for (top) TES CO retrievals and (bottom) TES-MLS joint CO retrievals between surface and 50 hPa, 9–10 Feb 2009.

to the north of New Zealand—not present in the a priori—stand out. MLS observed CO at 215 hPa also shows very high VMRs at a similar location. As we mentioned before, this enhanced upper tropospheric CO is due to known bush fire sources over SE Australia. MLS 215 hPa CO also shows enhancements in the convective tropics. For this single day at 215 hPa, MLS CO map shows much larger variability over the globe compared to TES. This is due to (1) TES CO retrieval being less sensitive in the upper troposphere, and (2) the two instrument teams using a different a priori profile and the constraints in their retrievals. The combined CO map keeps the major features in the distribution common in both TES and MLS stand-alone retrievals. As described in section 3.2, we adjusted the original MLS retrieval constraints for pressures greater than 100 hPa in this joint TES-MLS retrieval in order to better match the CO profile at lower altitudes to the stand-alone TES observations, for which a tighter constraint is used.

[27] The percent differences between TES-MLS combined CO VMRs and those of TES and MLS original products at 215 hPa are shown in Figure 10. The global distributions in the percent difference maps appear random. No systematic patterns are seen. This indicates that the combined retrieval does not introduce biases. The slight higher CO values in the combined product over tropical and midlatitude regions compared to the stand-alone TES observations (dominated

by the a priori state) is due to added sensitivity in CO retrievals introduced by adding MLS measurements. The larger standard deviation in combined and MLS comparisons (Figure 10, bottom) indicates that a tighter constraint is applied in the combined product.

[28] At 681 hPa (Figure 11), the combined CO distribution is very similar to that of TES as expected, since MLS CO measurements are used only at tangent pressures less than 316 hPa. Compared to TES, there are some minor differences in combined CO at 681 hPa. We see slightly higher variability and higher CO VMR at locations to the north of New Zealand, likely resulting from the weaker constraint in combined CO retrievals compared to that of TES. The CO VMRs at lower pressure levels influence the retrieved CO values at 681 hPa. This effect is demonstrated by the averaging kernels shown in Figure 7.

[29] The degree of freedom for signal calculated for a retrieved species profile represents the number of independent pieces of information that the retrieval system obtains. Here we focus on the troposphere and lower stratosphere, where the combined CO retrievals gain most from the combination of TES and MLS measurements. Figure 12, top shows the TES total DOFS and TES-MLS combined CO DOFS between the surface and 50 hPa (Figure 12, bottom). The stand-alone TES CO retrieval has no information in the stratosphere; its total DOFS is therefore the same as tropospheric DOFS [Luo *et al.*, 2007a]. TES CO DOFSs are less than 2. The TES-MLS combined CO DOFSs below 50 hPa are 2.5–4, an improvement over TES-alone, mostly in upper troposphere and lower stratosphere. This much improved CO profile retrieval provides a unique data set for studying troposphere-stratosphere exchanges that are not available from a single nadir-viewing instrument.

[30] We picked a single TES-MLS pair to illustrate the original and the combined CO profiles. The TES and MLS locations for this profile pair are marked in Figure 4 in triangle, a scene with enhanced CO at 215 hPa observed by both instruments in the Australia bush fire plume. Figure 13, top shows the TES and MLS retrieved profiles, the a priori profile, and the combined TES-MLS CO profile. Both TES and MLS retrievals show unusually high CO in the upper troposphere originating from the SE Australia bush fires. The air was uplifted and traveled eastward [Pumphrey *et al.*, 2011]. The combined CO profile retained this enhanced upper-tropospheric layer. Figure 13, bottom show the a priori and the estimated retrieval errors, and the averaging kernels for the entire atmosphere and surface to 50 hPa, respectively. The total retrieval error for this case is less than 20 ppb, a reasonable reduction from the a priori uncertainty of 30–40 ppb for the most of the troposphere. Similar to the stand-alone TES profiles (not shown), the peak of the averaging kernels for the combined CO in the lower midtroposphere is 400–500 hPa. The largest improvement in averaging kernels compared to TES is in the upper troposphere and lower stratosphere where MLS measurements add significant information.

5. A Single Case Validation

[31] Here we use a single case comparison of satellite CO profile retrievals to the in situ measurements using the proper comparison method. In addition to illustrate the influences of

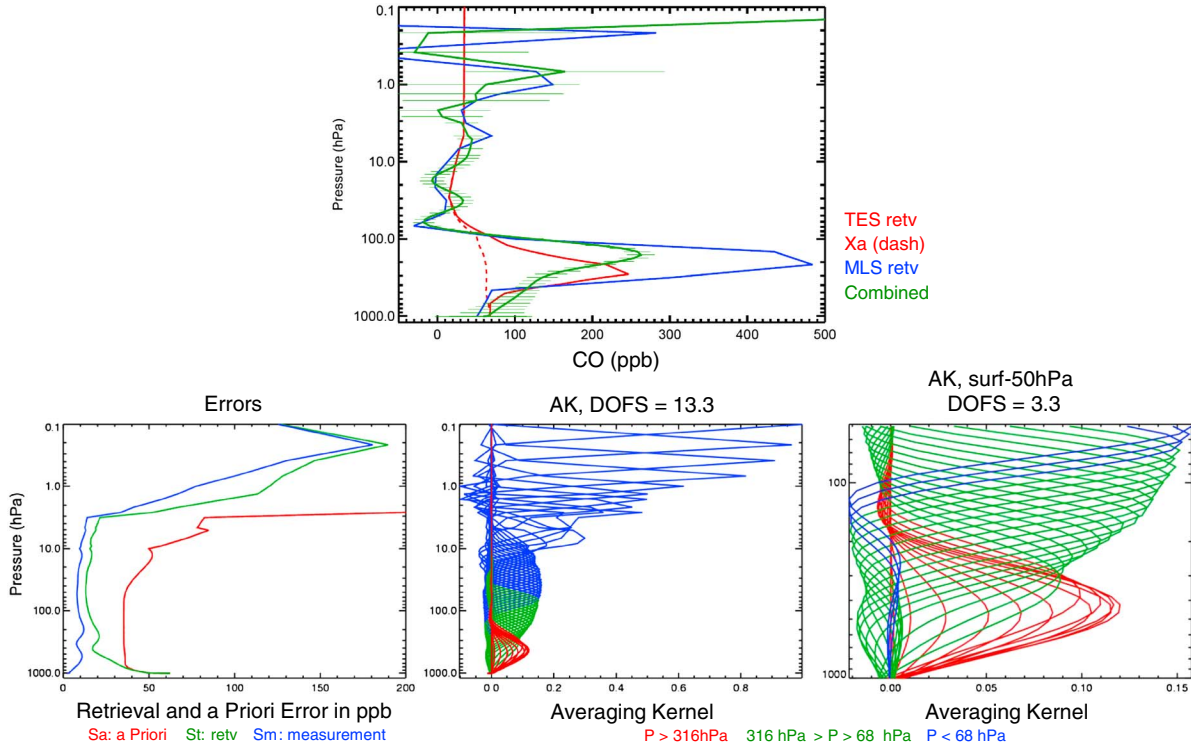


Figure 13. An example of TES-MLS CO profile retrieval. The locations are marked in Figure 4 in triangles. (top) The CO profiles: a priori (dotted red), TES alone retrieval (red), MLS alone retrieval (blue), and TES-MLS combined retrieval (green) with error bars. (bottom left) The plot for a priori error (red) and total retrieval error (green) profiles. (bottom middle) The averaging kernels for the entire atmosphere and (bottom right) between surface and 50 hPa.

the a priori to the satellite retrieved results, this case provides a preliminary validation to the TES-MLS combined CO product and the advantage of the combined product over the two stand-alone products.

[32] For the purpose of validating TES-MLS jointly retrieved CO profiles and other Aura products, balloon launches of the AirCore instrument are conducted on the Great Plains to the east of Denver, Colorado. The AirCore system collects air samples during the descending path of a balloon flight, and the samples are analyzed using Trace gas analyzers in the laboratory [Karion *et al.*, 2010]. In 2012, two AirCore balloon flights were conducted nearly coincident with a TES Stare (at MLS tangent) and a MLS observation. We show an example comparison taken 11 Oct 2012. The AirCore instrument descended from 50 hPa about 30 min after TES and MLS overpasses to the east of Denver and drifted ~40 km NE before landing. The weather for the day was mostly clear.

[33] Figure 14 shows the comparisons among AirCore, TES, MLS, and TES-MLS combined CO profiles. Unlike Figures 7 and 8, here the TES or MLS-alone results are those from the current standard products provided by the two instrument teams. The AirCore CO measurements (black dots) provide accuracies of 4 ppb. TES instrument (solid red) and the TES-MLS combined retrievals (solid green) in the lower midtroposphere roughly follow the profile with a nearly constant vertical gradient, indicating the effects of the level-correlated constraint. The MLS instrument retrievals (solid blue) above 215 hPa show large variability. In 200–50 hPa range, TES-MLS combined CO

agrees with AirCore very well while TES CO mostly follows that of the a priori profile.

[34] To properly compare the satellite profile retrievals and the in situ profile [Rodgers and Connor, 2003; Luo *et al.*, 2007b]. In Figure 14, the purple line shows the AirCore CO adjusted with TES-MLS combined averaging kernels, and the orange line shows the AirCore CO adjusted with TES averaging kernels. Due to gained information by adding MLS measurements, the combined result (purple) is different from the TES-alone result (orange). In the lower midtroposphere (surface to ~350 hPa), the difference between TES-MLS CO (green) and the adjusted AirCore (purple) and the difference between TES-alone CO (red) and the adjusted AirCore (orange) are similar. For pressures 350–150 hPa, TES-alone (red) and the adjusted AirCore (orange) appear to agree better than TES-MLS (green) and the adjusted AirCore (purple) comparison. This is due to the drop-off of TES sensitivity in the upper troposphere (see Figure 7 and discussions of section 3.4). In all pressure levels, the variability of TES-MLS retrieval is greater than that of TES due to the slight looser constraint used for the combined product described here compared to the one used by the TES instrument team. The lack of sensitivity of TES-alone retrievals is more obvious in the comparisons in 150–50 hPa range, where TES-MLS retrievals (green) closely follow the measured (black dots) and the adjusted (purple) AirCore CO, while TES-alone retrieval (red) and the adjusted AirCore CO closely follow the a priori (red dash).

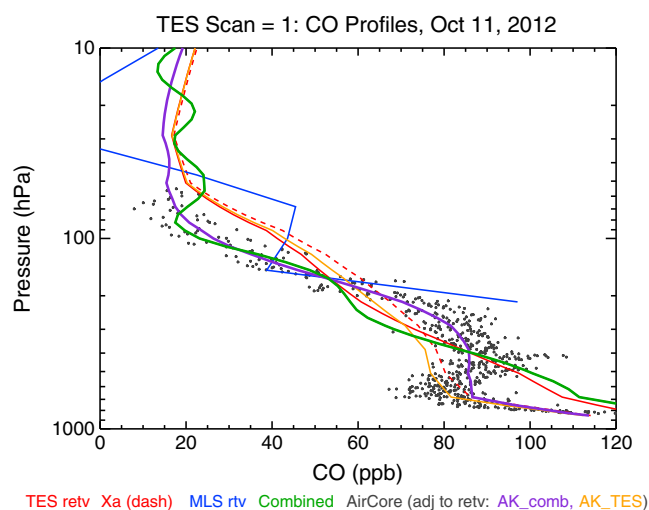


Figure 14. CO VMR profile comparisons among AirCore measurements (black dots), the a priori profile Xa (red dash), TES retrievals (solid red), MLS retrievals (solid blue), TES-MLS combined retrievals (solid green), and the AirCore profile adjusted by TES averaging kernel (orange) and TES-MLS combined averaging kernel (purple).

[35] More colocated comparisons are needed to draw statistical conclusions on the accuracies of the satellite retrievals. The agreement between TES-MLS jointly retrieved CO profile and the in situ measurements will be evaluated against measurement errors.

6. Summary and Future Work

[36] Atmospheric CO profiles are obtained from TES nadir and MLS limb observations on the Aura satellite. Their sensitivities are limited to the lower to middle troposphere for TES and higher up for MLS. Here we present the algorithm and retrieval results combining the closest TES nadir and MLS limb radiometric measurements to derive a single CO profile. In the upper troposphere where the TES CO retrieval sensitivity is low and MLS CO retrieval is near its lower cutoff boundary, the joint retrieval greatly improves retrieved CO profile over those retrieved by a stand-alone instrument. This CO data set should provide a new data source especially useful in studies of global air exchanges between the troposphere and stratosphere.

[37] We describe the processes in combining TES and MLS data and retrieving CO profiles. TES and MLS measurement pairs are found closest in time and location for TES global surveys. These pairs are within 7 ± 0.3 min and 50–220 km. MLS forward model results and TES prestored forward model data are optimally combined in retrieving a joint CO profile with the common a priori constraints. Averaging kernel and total retrieval error are calculated to characterize the retrieved results. We illustrated an example of combined CO data. The DOFS for the combined CO is 2.5–4 between surface and 50 hPa, a big improvement over TES DOFS of < 2 . In the lower troposphere, the combined CO global distribution is similar to that of TES; in the upper troposphere, the combined CO keeps the morphology from TES and MLS. With a tightened constraint, the combined CO field at 215 hPa shows less variability compared to that of MLS.

[38] The TES-MLS combined CO profile retrieval will be processed for the entire Aura mission and the data will be made available to the public. Validation of this CO product focusing on upper troposphere/lower stratosphere will be performed using the aircraft data, e.g., MOZAIC, INTEX-B, HIPPO campaigns.

[39] **Acknowledgments.** We would like to thank the strong support from the Aura project, TES and MLS teams. We thank the AirCore team for conducting the balloon flights and providing the analyzed CO data to support this project. The research described in this paper was carried out at the Jet Propulsion Laboratory, California Institute of Technology, under a contract with the National Aeronautics and Space Administration.

References

- Aumann, H. H., et al. (2003), AIRS/AMSU/HSB on the Aqua mission: Design, science objectives, data products, and processing systems, *IEEE Trans Geosci Remote Sens.*, *41*, 253–64.
- Barret, B., S. Turquety, D. Hurtmans, C. Clerbaux, J. Hadji-Lazaro, I. Bey, M. Auvray, and P.-F. Coheur (2005), Global carbon monoxide vertical distributions from spaceborne high-resolution FTIR nadir measurements, *Atmos. Chem. Phys.*, *5*, 2901–2914.
- Beer, R., T. A. Glavich, and D. M. Rider (2001), Tropospheric emission spectrometer for the Earth Observing System's Aura satellite, *Applied Optics*, *40*(15).
- Beer, R. (2006), TES on the Aura mission: Scientific objectives, measurements, and analysis overview, *IEEE Trans. Geosci. Remote Sens.*, *44*, 1102–1105.
- Bovensmann, H., J. P. Burrows, M. Buchwitz, J. Frerick, S. Noel, V. V. Rozanov, K. V. Chance, and A. P. H. Goede (1999), SCIAMACHY: Mission objectives and measurement modes, *J. Atmos. Sci.*, *56*, 125–150.
- Bowman, K. W., et al. (2006), Tropospheric emission spectrometer: Retrieval method and error analysis, *IEEE Trans. Geosci. Remote Sens.*, *44*, 1297–1307.
- de Laat, A. T. J., D. C. Stein Zweers, R. Boers, and O. N. E. Tuinder (2012), A solar escalator: Observational evidence of the self-lifting of smoke and aerosols by absorption of solar radiation in the February 2009 Australian Black Saturday plume, *J. Geophys. Res.*, *117*, D04204, doi:10.1029/2011JD017016.
- Edwards, D. P., et al. (2004), Observations of carbon monoxide and aerosols from the Terra satellite: Northern Hemisphere variability, *J. Geophys. Res.*, *109*, D24202, doi:10.1029/2004JD004727.
- Filipiak, M. J., R. S. Harwood, J. H. Jiang, Q. Li, N. J. Livesey, G. L. Manney, W. G. Read, M. J. Schwartz, J. W. Waters, and D. L. Wu (2005), Carbon monoxide measured by the EOS microwave limb sounder on Aura: First results, *Geophys. Res. Lett.*, *32*, L14825, doi:10.1029/2005GL022765.
- George, M., et al. (2009), Carbon monoxide distributions from the IASI/METOP mission: Evaluation with other space-borne remote sensors, *Atmos. Chem. Phys.*, *9*, 8317–8330.
- Glatthor, N., et al. (2013), The Australian bushfires of February 2009: MIPAS observations and GEM-AQ model results, *Atmos. Chem. Phys.*, *13*, 1637–1658, doi:10.5194/acp-13-1637-2013.
- Gonzi, S., and P. I. Palmer (2010), Vertical transport of surface fire emissions observed from space, *J. Geophys. Res.*, *115*, D02306, doi:10.1029/2009JD012053.
- Herman, R. L., and G. Osterman (Eds.) (2012), Tropospheric Emission Spectrometer Data Validation Report, D-33192, version 5.0, Jet Propul. Lab., California Institute of Technology, Pasadena, Calif. [available online at <http://tes.jpl.nasa.gov/documents>.]
- Herman, R. L., and S. S. Kulawik (Eds.) (2013), Tropospheric Emission Spectrometer TES Level 2 (L2) data user's guide, D-38042, version 5.0, Jet Propulsion Laboratory, California Institute of Technology, Pasadena, CA, available online at <http://tes.jpl.nasa.gov/documents>.
- Ho, S., D. P. Edwards, J. C. Gille, M. Luo, G. B. Osterman, S. S. Kulawik, and H. Worden (2009), A global comparison of carbon monoxide profiles and column amounts from Tropospheric Emission Spectrometer (TES) and Measurements of Pollution in the Troposphere (MOPITT), *J. Geophys. Res.*, *114*, D21307, doi:10.1029/2009JD012242.
- Jiang, J. H., N. J. Livesey, H. Su, L. Neary, J. C. McConnell, and N. A. Richards (2007), Connecting surface emissions, convective uplifting, and long-range transport of carbon monoxide in the upper-troposphere: New observations from the Aura Microwave Limb Sounder, *Geophys. Res. Lett.*, *34*, L18812, doi:10.1029/2007GL030638.
- Karion, A., C. Sweeney, P. Tans, and T. Newberger (2010), AirCore: An innovative atmospheric sampling system, *J. Atmos. Oceanic Technol.*, *27*, 1839–1853.

- Li, Q. B., et al. (2005), Convective outflow of South Asian pollution: A global CTM simulation compared with EOS MLS observations, *Geophys. Res. Lett.*, *32*, L14826, doi:10.1029/2005GL022762.
- Liu, J., J. A. Logan, D. B. A. Jones, N. J. Livesey, I. Megretskaya, C. Carouge, and P. Nédélec (2010), Analysis of CO in the tropical troposphere using Aura satellite data and the GEOS-Chem model: Insights into transport characteristics of the GEOS meteorological products, *Atmos. Chem. Phys.*, *10*, doi:10.5194/acp-10-12207-2010.
- Livesey, N. J., W. V. Snyder, W. G. Read, and P. A. Wagner (2006), Retrieval algorithms for the EOS Microwave Limb Sounder (MLS) instrument, *IEEE Trans. Geosci. Remote Sens.*, *44*(5), 1144–1155.
- Livesey, N. J., et al. (2008), Validation of Aura Microwave Limb Sounder O₃ and CO observations in the upper troposphere and lower stratosphere, *J. Geophys. Res.*, *113*, D15S02, doi:10.1029/2007JD008805.
- Livesey, N. J., et al. (2011), Version 3.3 level 2 data quality and description document, http://mls.jpl.nasa.gov/data/v3-3_data_quality_document.pdf.
- Logan, J., et al. (1981), Tropospheric chemistry: A global perspective, *J. Geophys. Res.*, *86*, 7210–7254.
- Logan, J. A., I. A. Megretskaya, R. Nassar, L. T. Murray, L. Zhang, K. W. Bowman, H. M. Worden, and M. Luo (2008), Effects of the 2006 El Niño on tropospheric composition as revealed by data from the Tropospheric Emission Spectrometer (TES), *Geophys. Res. Lett.*, *35*, L03816, doi:10.1029/2007GL031698.
- Lopez, J. P., M. Luo, L. E. Christensen, M. Loewenstein, H. Jost, C. R. Webster, and G. Osterman (2008), TES carbon monoxide validation during two AVE campaigns using the Argus and ALIAS instruments on NASA's WB-57F, *J. Geophys. Res.*, *113*, D16S47, doi:10.1029/2007JD008811.
- Luo, M., et al. (2007a), Comparison of carbon monoxide measurements by TES and MOPITT: Influence of a priori data and instrument characteristics on nadir atmospheric species retrievals, *J. Geophys. Res.*, *112*, D09303, doi:10.1029/2006JD007663.
- Luo, M., et al. (2007b), TES carbon monoxide validation with DACOM aircraft measurements during INTEX-B 2006, *J. Geophys. Res.*, *112*, D24S48, doi:10.1029/2007JD008803.
- Luo, M., C. Boxe, J. Jiang, R. Nassar, and N. Livesey (2010), Interpretation of Aura satellite observations of CO and aerosol index related to the December 2006 Australia fires, *Remote Sens. Environ.*, doi:10.1016/j.rse.2010.07.003.
- Nassar, R., J. A. Logan, I. A. Megretskaya, L. T. Murray, L. Zhang, and D. B. A. Jones (2009), Analysis of tropospheric ozone, carbon monoxide and water vapor during the 2006 El Niño using TES observations and the GEOS-Chem model, *J. Geophys. Res.*, *114*, D17304, doi:10.1029/2009JD011760.
- Pumphrey, H. C., et al. (2007), Validation of middle-atmosphere carbon monoxide retrievals from MLS on Aura, *J. Geophys. Res.*, *112*, D24S38, doi:10.1029/2007JD008723.
- Pumphrey, H. C., M. L. Santee, N. J. Livesey, M. J. Schwartz, and W. G. Read (2011), Microwave Limb Sounder observations of biomass-burning products from the Australian bush fires of February 2009, *Atmos. Chem. Phys.*, *11*(2), 6285–6296, doi:10.5194/acp-11-6285-2011.
- Read, W. G., Z. Shippony, M. J. Schwartz, N. J. Livesey, and W. V. Snyder (2006), The clear-sky unpolarized forward model for the EOS Microwave Limb Sounder (MLS), *IEEE Trans. Geosci. Remote Sens.*, *44*(5), 1367–1379.
- Rodgers, C. D. (2000), *Inverse Methods for Atmospheric Sounding: Theory and Practice*, World Sci., Hackensack, N. J.
- Rodgers, C. D., and B. J. Connor (2003), Intercomparisons of remote sounding instruments, *J. Geophys. Res.*, *108*(D3), 4116, doi:10.1029/2002/JD002299.
- Schoeberl, M. R., et al. (2006), Overview of the EOS Aura mission, *IEEE Trans. Geosci. Remote Sens.*, *44*(5), 1066–1074.
- Schoeberl, M. R., et al. (2008), QBO and annual cycle variations in tropical lower stratosphere trace gases from HALOE and Aura MLS observations, *J. Geophys. Res.*, *113*, D05301, doi:10.1029/2007JD008678.
- Siddaway, J. M., and S. V. Petelina (2011), Transport and evolution of the 2009 Australian Black Saturday bushfire smoke in the lower stratosphere observed by OSIRIS on Odin, *J. Geophys. Res.*, *116*, D06203, doi:10.1029/2010JD015162.
- Waters, J. W., et al. (2006), The Earth Observing System Microwave Limb Sounder (EOS MLS) on the Aura satellite, *IEEE Trans. Geosci. Remote Sens.*, *44*(5), 1075–1092.
- Zhang, L., et al. (2006), Continental outflow of ozone pollution as determined by O₃-CO correlations from the TES satellite instrument, *Geophys. Res. Lett.*, *33*, L18804, doi:10.1029/2006GL026399.
- Zhang, L., Q. Li, J. Jin, H. Liu, N. Livesey, J. H. Jiang, Y. Mao, D. Chen, M. Luo, and Y. Chen (2011), Impacts of 2006 Indonesian fires and dynamics on tropical upper tropospheric carbon monoxide and ozone, *Atmos. Chem. Phys.*, *11*, 1–18, doi:10.5194/acp-11-1-2011.